AIMS Materials Science, 12(5): 1025–1040.
DOI: 10.3934/matersci.2025047
Received: 06 July 2025
Revised: 17 September 2025
Accepted: 10 October 2025
Published: 20 October 2025

https://www.aimspress.com/journal/Materials

Research article

Tailoring mechanical and functional properties of calcium sulphoaluminate cement (CSA) foam concrete with FA and GGBS replacements

Yun-Lin Liu[1], Xing-Zheng Xiao[2], Xing-Yu Zhou[3], Lan-Ping Qian[4] and Dong Guo[5,*]

[1] Prefabricated Building Research Institute of Anhui Province, Anhui Jianzhu University, Hefei, China
[2] School of Civil Engineering, Anhui Jianzhu University, Hefei, China
[3] Anhui Construction Engineering Inspection Technology Group Co., Ltd, Hefei, China
[4] Faculty of Architecture, Civil and Transportation Engineering, Beijing University of Technology, Beijing, China
[5] School of Civil Engineering and Transportation, Guangzhou University, Guang Zhou, China

* **Correspondence:** Email: dong.ce.guo@connect.polyu.hk.

Abstract: Calcium sulphoaluminate cement (CSA) has been recognized for its rapid hardening, high early strength, strong chloride resistance, and low carbon emissions. This study developed a CSA-based foam concrete using a physical foaming method, incorporating industrial by-products—fly ash (FA) and ground granulated blast-furnace slag (GGBS)—at replacement ratios of 0%–30% to reduce costs and modify properties. Key properties assessed were flowability, dry shrinkage, density, compressive strength, and thermal conductivity. Results showed that FA and GGBS enhance flowability, reduce dry shrinkage and density, and diminish compressive strength, with dosage-dependent effects. The optimal replacement ratio of FA was 15%, yielding the lowest thermal conductivity at 0.0638 W/m·K, with only a minor strength reduction relative to the pure CSA foam concrete. The findings enable tailored design of sustainable, cost-effective CSA foam concrete using industrial by-products.

Keywords: foam concrete; calcium sulphoaluminate cement; fly ash; ground granulated blast-furnace slag

1. Introduction

Foam concrete has gained significant traction in construction due to its distinct advantages over traditional concrete, including reduced density, enhanced thermal insulation, and improved resistance to dynamic loading [1–5]. These properties are attributed to the closed-cell pore structure within the concrete, achieved through either chemical or physical foaming methods. While ordinary Portland cement (OPC) remains the predominant binder for foam concrete, its production raises substantial environmental concerns, accounting for approximately 8% of global anthropogenic CO_2 emissions [3] and generating other pollutants [6]. To address these issues, calcium sulfoaluminate cement (CSA) has emerged as a sustainable alternative. Research indicates that CSA concrete exhibits lower shrinkage [7], accelerated strength development [8,9], and superior sulfate resistance compared with OPC concrete [7,10]. These advantages make CSA particularly suitable for urgent repairs and sub-zero temperature applications, and these advantages also apply to CSA foam concrete [11].

To further enhance the sustainability and performance of CSA concrete, supplementary cementitious materials such as fly ash (FA) and ground granulated blast-furnace slag (GGBS) have been incorporated as partial replacements for CSA [12]. As industrial by-products, these materials offer substantial cost reductions [13–17] while amplifying the environmental benefits of CSA [18,19]. In addition, FA and GGBS are two of the most widely produced industrial by-products worldwide. The global annual output of fly ash is approximately 800–900 million tons, and slag output reaches 300–360 million tons [20]. In industrial regions such as China, India, the United States, and Europe, supplies of these materials are abundant and stable, providing a reliable supply channel for use in building materials. Their inclusion improves workability, reduces heat of hydration (mitigating thermal cracking) [21], and modulates early strength development while promoting long-term strength through pozzolanic and hydraulic reactions [21,22]. Furthermore, FA and GGBS also contribute to a denser hardened cement paste microstructure, which decreases permeability and enhances durability by limiting the ingress of deleterious agents [23]. However, the properties and replacement ratios of FA and GGBS require careful consideration, as they significantly influence both fresh and hardened concrete properties [12].

At the mesoscale, foam concrete is a two-phase material consisting of a cementitious matrix and entrained pores. Its functional properties (e.g., thermal conductivity, sound absorption) and mechanical properties (e.g., compressive strength, flexural strength) depend on both matrix characteristics (e.g., compressive strength, thermal conductivity) and pore characteristics (e.g., porosity, pore size distributions, average pore size, and roundness) [24–26]. Hilal et al. [27] reported a near-linear relationship between the compressive strength of foam concrete and its matrix strength. Similarly, lower thermal conductivity in the matrix yields better insulation in foam concrete [28]. Pore characteristics—porosity, average pore size, and roundness—also critically affect performance; higher porosity and larger pore size reduce density and compressive strength [27–31], while increased porosity generally lowers thermal conductivity [28].

Both physical (mechanical) [28,32–34] and chemical methods [30,35–37] are used to entrain pores in foam concrete. Physical methods involve blending pre-generated foam (produced using foaming agents [38]) with cement slurry. Common foaming agents include protein-based (e.g., hydrolyzed keratin from hooves/horns), synthetic, hydrolyzed proteins, and plant-derived types (e.g., saponins from soapberry or yucca) [26,39]. Animal keratin-based agents denature during air incorporation,

forming stable films around bubbles, resulting in high-quality foam that enhances concrete strength and durability [39].

Based on the above, the addition of FA and GGBS can modify the fresh and hardened properties of CSA paste. However, their specific impact on the mesoscale structure and performance of CSA foam concrete remains largely unexplored. This gap hinders the optimization and sustainable design of CSA foam concrete. The vast majority of existing research focuses on traditional OPC systems or pure CSA systems. This study is the first to systematically incorporate large amounts of solid waste (FA and GGBS) into a CSA cement-based foam concrete system. In addition, a detailed investigation was conducted on their synergistic effects on workability, hydration process, pore structure, and macroscopic properties. This study aims to enable the design of enhanced, cost-effective, and environmentally sustainable CSA foam concretes by leveraging industrial by-products.

2. Materials and methods

2.1. Materials

Class F FA and S95-grade GGBS were obtained from Henan Yulian Energy Co., Ltd. and from Tangshan Iron and Steel Co., Ltd., respectively. The same batches of material were also utilized as precursors for geopolymer foam concrete in the authors' previous study [25]. FA and GGBS were chosen based on a comprehensive assessment that included their high chemical complementarity with CSA, their synergistic performance, abundant and stable supply sources, and their conceptual compliance with the circular economy [40,41]. The Brunauer–Emmett–Teller (BET) specific surface areas of FA, CSA, and GGBS were measured to be 0.37, 2.38, and 1.34 m^2/g, respectively. Their chemical compositions were determined through X-ray fluorescence (XRF) analysis and are presented in Table 1. A naphthalene-based superplasticizer (FDN-C) was chosen for its high water-reduction capacity (15%–25%) and proven compatibility with CSA systems.

Table 1. Chemical compositions of FA, GGBS, and CSA by XRF (%).

	SiO_2	Al_2O_3	CaO	Fe_2O_3	K_2O	MgO	TiO_2	SO_3	Na_2O
CSA	12.52	25.53	42.31	3.12	-	2.01	-	11.96	-
FA	54.97	33.90	3.38	2.05	1.46	1.11	1.02	0.89	0.55
GGBS	31.24	16.92	39.41	-	0.35	7.97	1.19	1.45	-

"–" indicates that the composition is below the detection limit.

An animal keratin-based foaming agent derived from hooves and horns served as the foaming agent. This agent reduces surface tension to facilitate stable air bubble entrapment during mixing [39,42]. The same type of foaming agent was adopted in previous tests in [26]. The stability of the produced foam was quantitatively assessed using the method specified in JG/T 266–2011. The foam was placed in a cylindrical vessel (height: 80 mm, diameter: 120 mm) and loaded with a 33.5 g steel plate. As a result, the foam exhibited a settling distance of only 2 mm after 1 h, confirming its high stability. Key properties provided by the manufacturer are summarized in Table 2.

Table 2. Properties of the foam stabilizer.

Product	Color	Density (g/mL)	Foam drainage (mm/L)	Drainage rate (%)	Dilution ratio (%)	Foaming ratio (%)
Animal protein foaming agent	Sepia	1.1	3.0	20.0	30.0	73.0

The mixture proportions for all specimens are detailed in Table 3. The replacement levels of FA and GGBS were investigated from 0% to 30% by CSA mass in 5% increments. This range encompasses the typical optimum replacement zone (20%–40%) for supplementary cementitious materials in cementitious systems [40,43–46], while providing adequate resolution to identify performance thresholds and optimization points for CSA-based foamed concrete [41,45]. The 5% increment balances experimental precision with practical feasibility. Specimens were labeled according to FA and GGBS replacement ratios (0%–30% by mass). For instance, "FA-15" denotes 15% CSA replacement by FA. All mixtures maintained a foam volume ratio of 73%.

Table 3. Mixture compositions of foam concrete.

Specimens	FA (g)	GGBS (g)	CSA (g)	Water (g)	Superplasticizer (g)
FA-0	0	0	795.14	596.36	7.95
FA-5	39.76	0	755.38	596.36	7.95
FA-10	79.51	0	715.63	596.36	7.95
FA-15	119.27	0	675.87	596.36	7.95
FA-20	159.03	0	636.11	596.36	7.95
FA-25	198.79	0	596.36	596.36	7.95
FA-30	238.54	0	556.60	596.36	7.95
GGBS-5	0	39.76	755.38	596.36	7.95
GGBS-10	0	79.51	715.63	596.36	7.95
GGBS-15	0	119.27	675.87	596.36	7.95
GGBS-20	0	159.03	636.11	596.36	7.95
GGBS-25	0	198.79	596.36	596.36	7.95
GGBS-30	0	238.54	556.60	596.36	7.95

2.2. Preparation of foam concrete

The process of preparing CSA foam concrete is depicted in Figure 1. Initially, the FDN-C and the proportioned water were blended for 120 s to achieve thorough dissolving. CSA and FA/GGBS were then dry mixed for 180 s. Concurrently, the foaming agent was diluted 25-fold with water and added to the foaming machine. The foam was generated through the action of a high-speed agitator, operating for 150 s at a speed of 1800 rpm. Fresh foam was incorporated into the slurry and blended for 60 s. The foam concrete slurry was then transferred into molds and covered with plastic wrap to inhibit water evaporation. After one day, the specimens were demolded and placed in a curing room maintained at 20 ± 2 °C and a relative humidity of 95%.

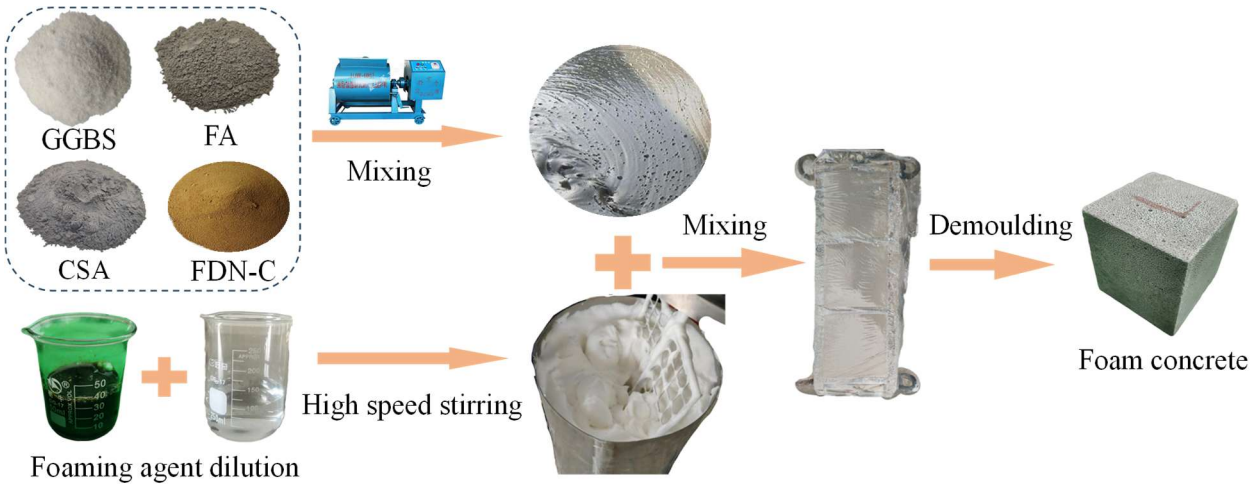

Figure 1. Preparation of CSA foam concrete.

2.3. Test methods

The flowability of the slurry was assessed according to the GB/T 2419-200 standard, using the flow table test for foam concrete. The test involves dampening the flow table and the inside of the cone mold to prevent the foam concrete from sticking. The cone mold was positioned at the center of the flow table and filled with foam concrete in two equal layers, with each layer compacted using a tamping rod. After compacting, the mold was carefully lifted vertically, allowing the foam concrete to spread, and the diameter of the spread foam concrete was measured in at least two directions.

The drying shrinkage of CSA foam concrete was tested in accordance with JGJ/T70-2009. The initial lengths of the foam concrete specimens were recorded after two days of curing. These lengths were measured again at predetermined intervals of 1, 3, 7, 14, and 28 days of curing, using a comparator to ensure precise measurements.

Density measurements for the foam concrete were conducted in line with JG/T266-2011, where three samples were prepared and oven-dried after a 28-day curing period. The density was then calculated by dividing the mass of each dried sample by its volume. The compressive strength was tested using a universal testing machine on 70.7 mm cubic specimens at a loading rate of 0.01 MPa/s, as stipulated in the JGJ/T70-2009 standard [47].

Thermal conductivity tests were carried out on 300 × 300 × 30 mm specimens, using a heat flow meter apparatus (DD300F-D15, Foreda), in accordance with GB/T 10295-2008. During the test, the hot and cold plates were placed on the opposite surfaces of the specimens. Thermal conductivity measurements commenced once steady-state conditions were achieved, as determined by the testing system through automatic verification that five consecutive thermal resistance readings (recorded at 300 s intervals) agreed within ±1% without monotonic directional change.

3. Results and discussion

Figure 2 demonstrates the variations in flowability of fresh CSA foam concrete with various FA and GGBS replacement ratios. According to the figure, the flowability of foam concrete gradually increased with the addition of FA, peaking at a 30% replacement ratio, exhibiting a value of 160 mm.

This enhancement is attributed to the spherical and relatively smooth nature of FA particles (median particle diameter is 14.2 μm [25]). These particles acted as miniature ball bearings within the mixture, reducing internal friction and thus improving the flowability as revealed by the scanning electron microscope (SEM) images in [48–50]. GGBS similarly improved flowability due to its finer particle size relative to sulphoaluminate cement (SAC). However, SEM observations of the same material batch [25] revealed that GGBS's angular morphology limits the relative sliding between slurry particles, thus its contribution to the flowability is minor compared to FA [50].

The improvement in flowability due to the addition of fly ash and GGBS can be particularly beneficial in foam concrete, as it facilitates the mixing and handling of the lightweight slurry, ensuring that the foam remains evenly distributed throughout the matrix and does not collapse during mixing and pouring [51,52].

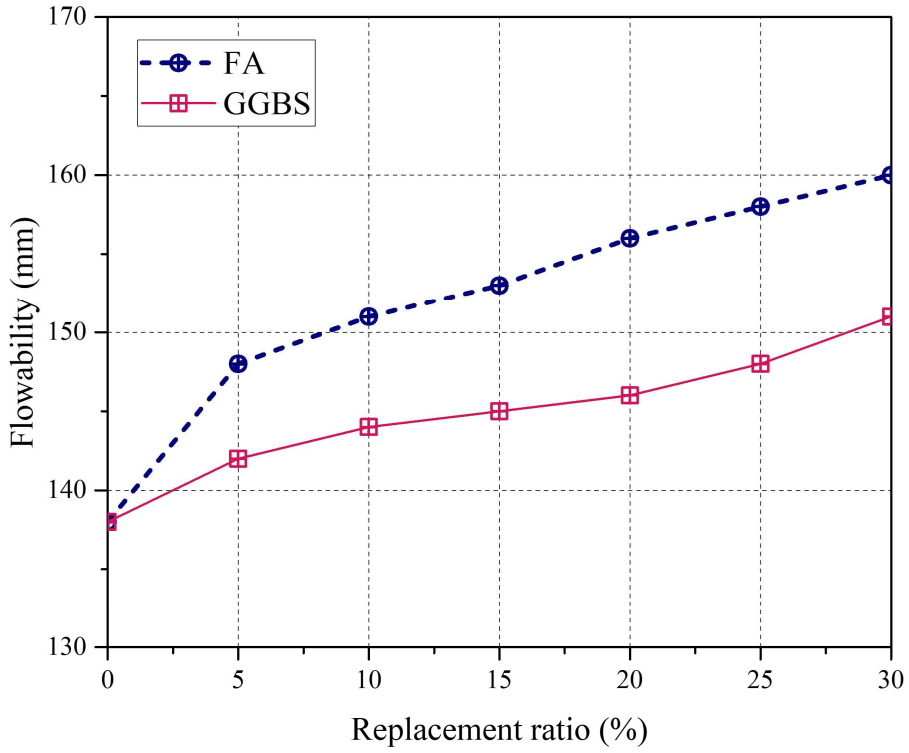

Figure 2. Effect of FA and GGBS replacement ratios on the flowability of CSA foam concrete.

Figure 3 demonstrates the variations of drying shrinkage of CSA foam concrete after curing for 3, 7, 14, and 28 days. It can be seen that the drying shrinkage of the CSA foam concrete was higher at longer curing ages and changed at different replacement ratios. The addition of FA and GGBS curtailed the dry shrinkage of foam concrete, and their contributions became more pronounced at longer drying times. This effect can be attributed to the reaction of silica content in FA and GGBS with CSA's hydration-released calcium hydroxide, which formed additional calcium silicate hydrate (C-S-H). This additional C-S-H formation reduced porosity and microcracking, thus diminishing shrinkage. In addition, their small particle size contributed to a denser, more homogenous microstructure by filling gaps between cement grains, which further mitigates shrinkage potential. Moreover, fly ash retains water, gradually releasing it for ongoing cement particle hydration. This internal curing effect maintains moisture within the concrete, reducing shrinkage through a more

uniform and extended hydration process [53]. As reported in [54] and [55], water retention is one of the most important reasons for explaining the observed significant reduction in dry shrinkage. This effect can be revealed through the strong positive correlation between drying shrinkage and moisture loss [56,57].

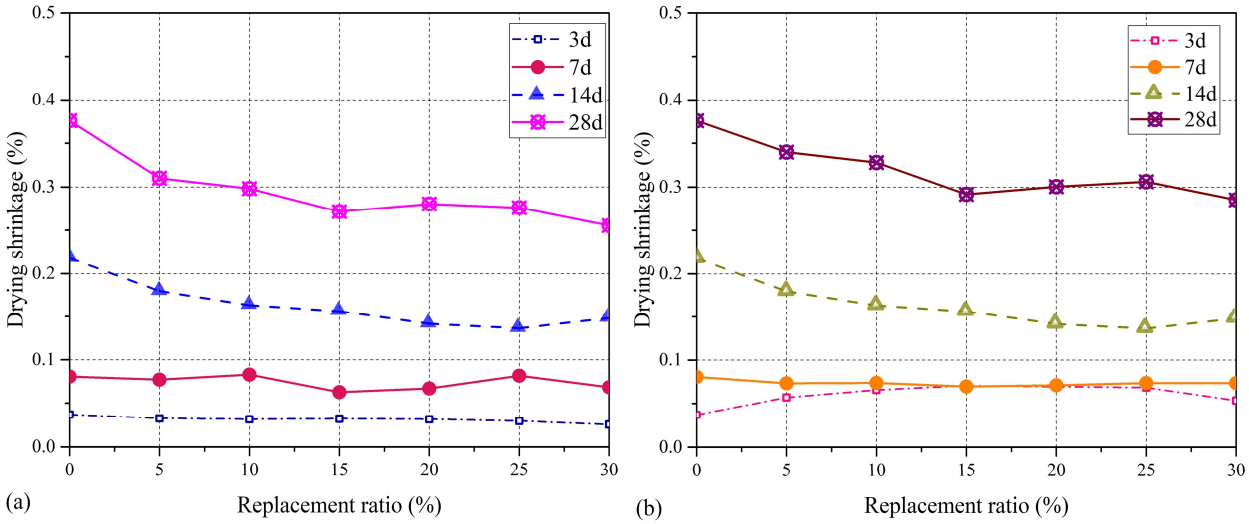

Figure 3. Effect of (a) FA and (b) GGBS replacement ratios on the shrinkage of CSA foam concrete.

Figure 4 illustrates the variations in the dry density of CSA foam concrete at different replacement ratios of FA and GGBS. The graph reveals that substituting CSA with GGBS or FA results in a decrease in foam concrete density. The specimens with FA replacements achieved their lowest density at a substitution rate of 25%, exhibiting a reduction ratio of 6.8% compared to the control specimens. In comparison, the density of specimens with slag is lowest at a substitution rate of 30% and 5.2% lower than the control group. This phenomenon can be attributed to the physical properties of these materials, their interactions within the concrete matrix, and the resultant characteristics of the pores. Generally, FA and GGBS possess lower specific gravities than CSA, leading to an overall reduction in mix density as the substituted materials are inherently lighter [58]. The interaction of FA and GGBS with calcium hydroxide, which forms additional C-S-H, might suggest a potential for a denser microstructure [58]. This is observable as a marginal density reduction at a 10% GGBS replacement level. However, the reactivity of FA and GGBS in the comparatively low alkaline environment of CSA is limited, resulting in a significant presence of unreacted FA and GGBS particles within the dense structures of CSA's hydration products. Furthermore, the enhanced flowability of the concrete mix (Figure 2) can unintentionally introduce larger air voids into the concrete structure, increasing the air void diameter and porosity of the foam concrete, as revealed by the micro-CT tests in [48].

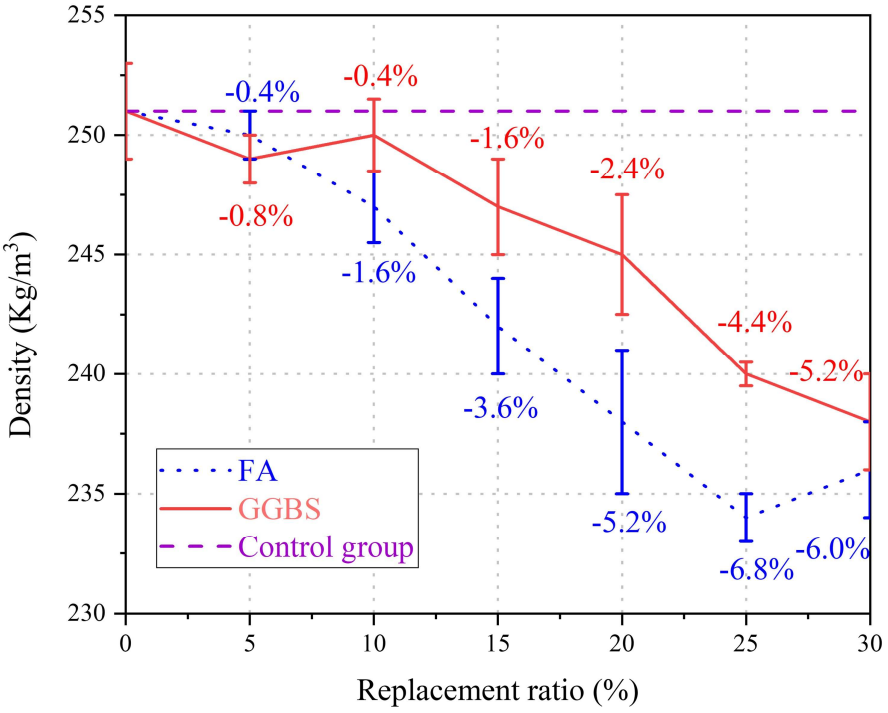

Figure 4. Effect of FA and GGBS replacement ratios on the dry density of CSA concrete.

Figure 5 illustrates the variations in compressive strength of CSA foam concrete at different FA/GGBS replacement ratios after curing for 7 and 28 days. It can be seen that the compressive strength gradually reduced with increasing FA and GGBS proportions. According to Figure 5a, the compressive strength reduction is relatively minor below 10% FA content. Yet, at a 15% FA content, there is a more noticeable decrease, with a 9.5% reduction at 7 days and a 5.6% decrease at 28 days. At a 30% FA replacement, the compressive strength plummets from 0.66 to 0.5 MPa at 7 days (a 24.2% reduction), and from 0.75 to 0.55 MPa at 28 days (a 27.7% reduction).

Figure 5b shows that increasing the GGBS replacement ratio continuously reduced the compressive strength of CSA foam concrete. Notably, at a 5% GGBS replacement, the strength significantly decreased, marking a 6.7% decrease at a 5% GGBS content. The compressive strength declined almost linearly with further GGBS content increase, dropping to 0.52 and 0.593 MPa at 7 and 28 days, respectively, at a 30% GGBS content.

This decrease in compressive strength can be attributed to the lower reactivity of FA and GGBS in the low alkaline environment of CSA paste, which reduced the strength of the pore walls. Previous reports stated that FA and GGBS's fine particles can fill voids between coarser cement particles for denser packing and a more uniform distribution [12], but their filling effect did not compensate for the strength loss due to their lower reactivity [12]. The reduction in compressive strength of the CAS paste was primarily explained by total porosity increasing from 26.1% to 35.4% and dominant pore sizes shifting beyond 100 nm, as measured by Mercury Intrusion Porosimetry (MIP) tests [46]. In addition, this microstructural deterioration can be compounded by decreased ettringite (AFt) formation, quantified through Thermogravimetry-Differential Scanning Calorimetry (TG-DSC) testing in [46]. Simultaneously, the dominance of dilution effects over pozzolanic activity above 10% GGBFS can be

attributed to CSA's limited calcium hydroxide production, which reduced overall hydration products, as evidenced by TG-DSC testing [46].

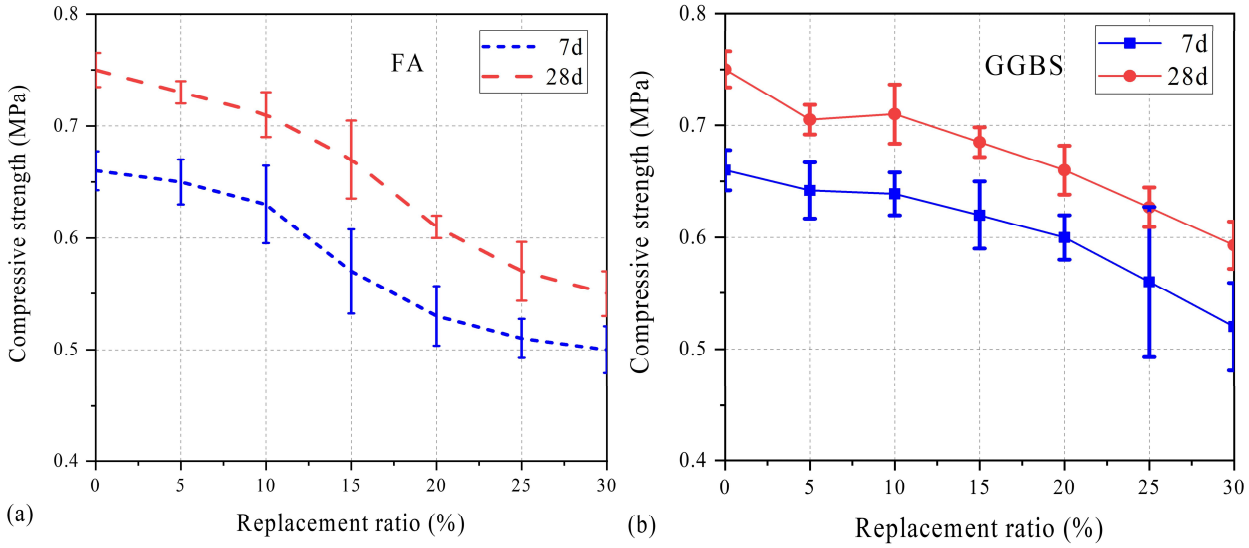

Figure 5. Effect of (a) FA and (b) GGBS replacement ratios on the compressive strength of CSA foam concrete.

Figure 6 illustrates how the thermal conductivity of CSA foam concrete varied with different ratios of FA or GGBS proportions. A distinct divergence in the effects of FA and GGBS substitutions on thermal conductivity was observed. According to Figure 6, the thermal conductivity coefficient of foam concrete exhibited a significant decrease with an increase in FA content up to 15%. At this FA content, the thermal conductivity dropped from 0.0784 W/(m·K) for pure CSA foam concrete to 0.0638 W/(m·K), indicating a notable improvement in thermal insulation. Beyond this point, the thermal conductivity stabilized, with values oscillating between 0.0638 and 0.0630 W/(m·K) for FA contents ranging from 15% to 30%. This trend confirms that FA inclusion is effective in reducing the thermal conductivity coefficient. The reduction can be attributed, in part, to the addition of unreacted FA particles, which contain spherical beads with low thermal conductivity that act as insulators within the matrix [59,60]. These particles replace other materials within the concrete that have higher thermal conductivity, thereby decreasing the overall heat transfer. Additionally, fly ash contributes to the loosening of the microstructure. Another contributing factor is the improved fluidity of the paste due to the FA addition, which facilitates the coalescence of smaller air bubbles into larger ones, increasing the pore size within the samples and slightly decreasing density (Figure 4), and enhancing the thermal insulation properties [61,62].

In contrast, when the proportion of GGBS in foam concrete was increased, there was a slight rise in thermal conductivity (Figure 6). This is somewhat counterintuitive, given that GGBS, with its higher reactivity compared to FA, engages in reactions with calcium hydroxide in the presence of water to form additional C-S-H gel. Such reactions typically lead to a denser concrete microstructure in the pore walls, which might be expected to lower thermal conductivity by reducing the pathways for heat transfer.

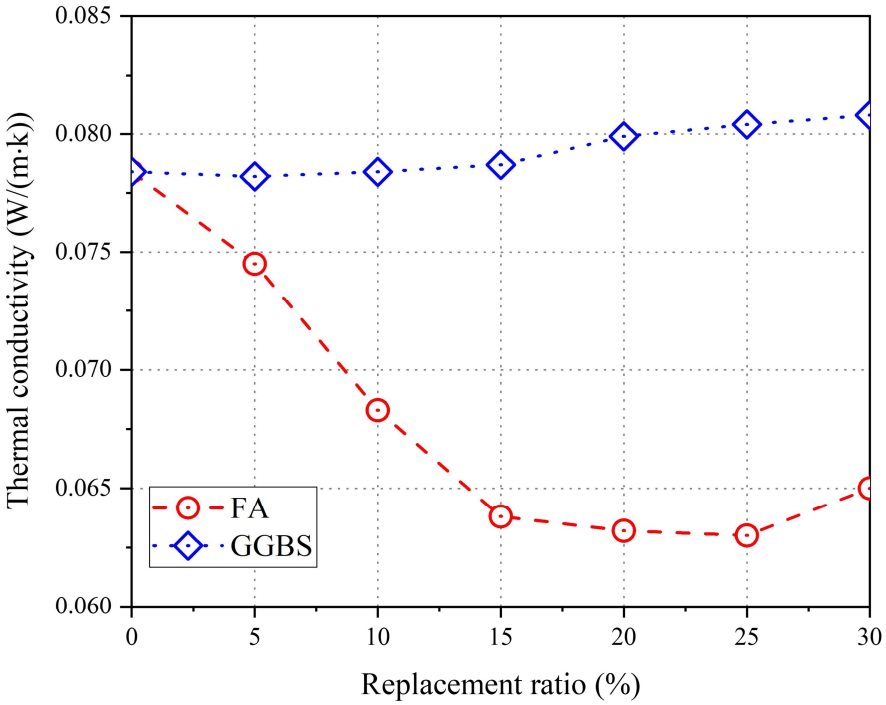

Figure 6. Effect of FA and GGBS replacement ratios on the thermal conductivity of CSA foam concrete.

The influence of GGBS on thermal conductivity is multifaceted. One key factor is the enhanced flowability of the CSA slurry at higher GGBS contents. While this improved flowability can be advantageous for the workability of the concrete, it also encourages the formation of larger voids or a more interconnected pore structure within the concrete matrix. This structural change can inadvertently increase thermal conductivity. The reasoning behind this is that larger, air-filled voids offer less resistance to heat flow compared to smaller, more isolated pores. Therefore, even as GGBS contributes to densifying the concrete's microstructure in the pore walls of foam concrete, through the formation of additional C-S-H, the resultant larger voids or channels within the matrix can enhance the material's overall thermal conductivity, illustrating the complex interplay between material composition, microstructural characteristics, and thermal properties in foam concrete.

4. Conclusions

This study explored the impact of varying proportions of FA and ground GGBS on the properties of CSA foam concrete, examining parameters such as workability, drying shrinkage, compressive strength, and thermal conductivity. The findings are summarized as follows:

(1) Both FA and GGBS admixtures improve the flowability of CSA foam concrete, with a more pronounced effect of FA.

(2) Both supplementary materials effectively mitigate drying shrinkage in ultra-lightweight foam concrete. At 28 days, the 30% GGBS replacement ratio yielded the lowest shrinkage, 12% lower than the pure CSA control mixture.

(3) Compressive strength decreases progressively with increasing FA or GGBS content across all curing ages. Strength reduction remains marginal (<10%) below 10% replacement but intensifies at higher dosages, with the 30% FA mix exhibiting the maximum strength reduction of 26.7%.

(4) Incorporation of 5%–15% FA significantly reduces thermal conductivity, decreasing from 0.0784 to 0.0683 W/(m·K) (12.9% reduction) at 15% replacement. Beyond this threshold, further thermal insulation improvement plateaus. Conversely, GGBS addition slightly increases thermal conductivity.

(5) These conclusions indicate that both FA and GGBS can be beneficially incorporated into CSA foam concrete, but their effects on the material properties are dosage-dependent. While FA is more effective in enhancing workability and reducing thermal conductivity, GGBS may be preferable for optimizing compressive strength while still improving workability and controlling shrinkage. The study provides a comprehensive understanding of how varying levels of these mineral admixtures influence the performance of CSA foam concrete, which can inform the design and optimization of this construction material for specific applications.

Use of AI tools declaration

The authors declare they have not used Artificial Intelligence (AI) tools in the creation of this article.

Acknowledgements

The authors would like to acknowledge the financial support received from National Natural Science Foundation of China (52408323); Anhui Provincial Universities Natural Science Research Project (KJ2020ZD43, 2022AH050261); the Department of Science and Technology of Guangdong Province, China (Project Nos. 2023A1515110842); Anhui Provincial Natural Science Foundation Project (1908085ME144); Doctoral Startup Foundation from Anhui Jianzhu University (2022QDZ23); Open Foundation of the Key Lab of Prefabricated Building Research Institute of Anhui Province (AHZPY2023KF02); the Guangdong Provincial Key Laboratory of Durability for Marine Civil Engineering Shenzhen Durability Center for Civil Engineering (Project No. GDDCE24-25-05).

Author contributions

Liu Yun-Lin: conceptualization, supervision; Xiao Xing-Zheng: writing—original draft, methodology, data curation; Zhou Xing-Yu: methodology; Qian Lan-Ping: project administration; Guo Dong: investigation, writing—review & editing; validation.

Conflict of interest

The authors declare no conflict of interest.

References

1. Ramamurthy K, Kunhanandan Nambiar EK, Indu Siva Ranjani G (2009) A classification of studies on properties of foam concrete. *Cement Concrete Comp* 31: 388–396. https://doi.org/10.1016/j.cemconcomp.2009.04.006

2. Terzi A, Pezo L, Miti V, et al. (2015) Artificial fly ash based aggregates properties influence on lightweight concrete performances. *Ceram Int* 41: 2714–2726. https://doi.org/10.1016/j.ceramint.2014.10.086
3. Sang G, Zhu Y, Yang G, et al. (2015) Preparation and characterization of high porosity cement-based foam material. *Constr Build Mater* 91: 133–137. https://doi.org/10.1016/j.conbuildmat.2015.05.032
4. Ding Z, Dong B, Xing F, et al. (2012) Cementing mechanism of potassium phosphate based magnesium phosphate cement. *Ceram Int* 38: 6281–6288. https://doi.org/10.1016/j.ceramint.2012.04.083
5. Bildirici ME (2019) Cement production, environmental pollution, and economic growth: Evidence from China and USA. *Clean Technol Envir* 21: 783–793. https://doi.org/10.1007/s10098-019-01667-3
6. Provis JL (2014) Geopolymers and other alkali activated materials: Why, how, and what? *Mater Struct* 47: 11–25. https://doi.org/10.1617/s11527-013-0211-5
7. Sirtoli D, Wyrzykowski M, Riva P, et al. (2019) Shrinkage and creep of high-performance concrete based on calcium sulfoaluminate cement. *Cement Concrete Comp* 98: 61–73. https://doi.org/10.1016/j.cemconcomp.2019.02.006
8. Zhang G, Yang Y, Yang H, et al. (2020) Calcium sulphoaluminate cement used as mineral accelerator to improve the property of Portland cement at sub-zero temperature. *Cement Concrete Comp* 106: 103452. https://doi.org/10.1016/j.cemconcomp.2019.103452
9. Shen Y, Qian J, Chai J, et al. (2014) Calcium sulphoaluminate cements made with phosphogypsum: Production issues and material properties. *Cement Concrete Comp* 48: 67–74. https://doi.org/10.1016/j.cemconcomp.2014.01.009
10. Ke G, Zhang J, Liu Y (2022) Shrinkage characteristics of calcium sulphoaluminate cement concrete. *Constr Build Mater* 337: 127627. https://doi.org/10.1016/j.conbuildmat.2022.127627
11. Li T, Huang F, Li L, et al. (2020) Preparation and properties of sulphoaluminate cement-based foamed concrete with high performance. *Constr Build Mater* 263: 120945. https://doi.org/10.1016/j.conbuildmat.2020.120945
12. García-Maté M, De la Torre A, León-Reina L, et al. (2013) Hydration studies of calcium sulfoaluminate cements blended with fly ash. *Cem Concr Res* 54: 12–20. https://doi.org/10.1016/j.cemconres.2013.07.010
13. Shang J, Dai JG, Zhao TJ, et al. (2018) Alternation of traditional cement mortars using fly ash-based geopolymer mortars modified by slag. *J Clean Prod* 203: 746–756. https://doi.org/10.1016/j.jclepro.2018.08.255
14. Qian LP, Xu LY, Alrefaei Y, et al. (2022) Artificial alkali-activated aggregates developed from wastes and by-products: A state-of-the-art review. *Resour Conserv Recy* 177: 105971. https://doi.org/10.1016/j.resconrec.2021.105971
15. Ahmad MR, Qian LP, Fang Y, et al. (2023) A multiscale study on gel composition of hybrid alkali-activated materials partially utilizing air pollution control residue as an activator. *Cement Concrete Comp* 136: 104856. https://doi.org/10.1016/j.cemconcomp.2022.104856
16. Wang YS, Alrefaei Y, Dai JG (2021) Roles of hybrid activators in improving the early-age properties of one-part geopolymer pastes. *Constr Build Mater* 306: 124880. https://doi.org/10.1016/j.conbuildmat.2021.124880

17. Wang YS, Alrefaei Y, Dai JG (2020) Influence of coal fly ash on the early performance enhancement and formation mechanisms of silico-aluminophosphate geopolymer. *Cem Concr Res* 127: 105932. https://doi.org/10.1016/j.cemconres.2019.105932
18. Cong M, Bing C (2015) Properties of a foamed concrete with soil as filler. *Constr Build Mater* 76: 61–69. https://doi.org/10.1016/j.conbuildmat.2014.11.066
19. Alrefaei Y, Wang YS, Dai JG, et al. (2020) Effect of superplasticizers on properties of one-part $Ca(OH)_2/Na_2SO_4$ activated geopolymer pastes. *Constr Build Mater* 241: 117990. https://doi.org/10.1016/j.conbuildmat.2019.117990
20. Scrivener K, Martirena F, Bishnoi S, et al. (2018) Calcined clay limestone cements (LC3). *Cem Concr Res* 114: 49–56. https://doi.org/10.1016/j.cemconres.2017.08.017
21. Poon CS, Kou S, Lam L, et al. (2001) Activation of fly ash/cement systems using calcium sulfate anhydrite ($CaSO_4$). *Cem Concr Res* 31: 873–881. https://doi.org/10.1016/S0008-8846(01)00478-1
22. Pan Z, Li H, Liu W (2014) Preparation and characterization of super low density foamed concrete from Portland cement and admixtures. *Constr Build Mater* 72: 256–261. https://doi.org/10.1016/j.conbuildmat.2014.08.078
23. Xue J, Li S, Zhang Z, et al. (2025) Hydration, mechanical properties, and corrosion resistance of ferroaluminate cement in the presence of FA and GGBS. *J Build Eng* 102: 111974. https://doi.org/10.1016/j.jobe.2025.111974
24. Muller AC, Scrivener KL, Gajewicz AM, et al. (2013) Densification of C–S–H measured by 1H NMR relaxometry. *J Phys Chem C* 117: 403–412. https://doi.org/10.1021/jp3102964
25. Liu YL, Liu C, Qian LP, et al. (2023) Foaming processes and properties of geopolymer foam concrete: Effect of the activator. *Constr Build Mater* 391: 131830. https://doi.org/10.1016/j.conbuildmat.2023.131830
26. Liu YL, Li CF, Zhai HX, et al. (2023) Production and performance of CO_2 modified foam concrete. *Constr Build Mater* 389: 131671. https://doi.org/10.1016/j.conbuildmat.2023.131671
27. Hilal AA, Thom NH, Dawson AR (2015) On void structure and strength of foamed concrete made without/with additives. *Constr Build Mater* 85: 157–164. https://doi.org/10.1016/j.conbuildmat.2015.03.093
28. Shao N, Zhang Y, Liu Z, et al. (2018) Fabrication of hollow microspheres filled fly ash based foam geopolymers with ultra-low thermal conductivity and relative high strength. *Constr Build Mater* 185: 567–573. https://doi.org/10.1016/j.conbuildmat.2018.07.077
29. Gu G, Xu F, Ruan S, et al. (2020) Influence of precast foam on the pore structure and properties of fly ash-based geopolymer foams. *Constr Build Mater* 256: 119410. https://doi.org/10.1016/j.conbuildmat.2020.119410
30. Dembovska L, Bajare D, Ducman V, et al. (2017) The use of different by-products in the production of lightweight alkali activated building materials. *Constr Build Mater* 135: 315–322. https://doi.org/10.1016/j.conbuildmat.2017.01.005
31. Liu Y, Huo S, Fu J, et al. (2024) Dynamic properties of CO_2-cured foam concrete at different loading rates: Effect of the foam admixtures and addition of polypropylene fiber. *Front Mater* 11: 1445848. https://doi.org/10.3389/fmats.2024.1445848
32. Al Bakri Abdullah MM, Hussin K, Bnhussain M, et al. (2012) Fly ash-based geopolymer lightweight concrete using foaming agent. *Int J Mol Sci* 13: 7186–7198. https://doi.org/10.3390/ijms13067186

33. Zhang Z, Provis JL, Reid A, et al. (2015) Mechanical, thermal insulation, thermal resistance and acoustic absorption properties of geopolymer foam concrete. *Cement Concrete Comp* 62: 97–105. https://doi.org/10.1016/j.cemconcomp.2015.03.013
34. Wang L, Tan X (2011) Preparation and properties of alkali activated foam cement reinforced with polypropylene fibers. *J WuHan Univ Technol* 26: 960–964. https://doi.org/10.1007/s11595-011-0345-7
35. Abdollahnejad Z, Pacheco-Torgal F, Félix T, et al. (2015) Mix design, properties and cost analysis of fly ash-based geopolymer foam. *Constr Build Mater* 80: 18–30. https://doi.org/10.1016/j.conbuildmat.2015.01.063
36. Hlaváček P, Šmilauer V, Škvára F, et al. (2015) Inorganic foams made from alkali-activated fly ash: Mechanical, chemical and physical properties. *J Eur Ceram Soc* 35: 703–709. https://doi.org/10.1016/j.jeurceramsoc.2014.08.024
37. Ducman V, Korat L (2016) Characterization of geopolymer fly-ash based foams obtained with the addition of Al powder or H_2O_2 as foaming agents. *Mater Charact* 113: 207–213. https://doi.org/10.1016/j.matchar.2016.01.019
38. Phavongkham V, Wattanasiriwech S, Cheng TW, et al. (2020) Effects of surfactant on thermo-mechanical behavior of geopolymer foam paste made with sodium perborate foaming agent. *Constr Build Mater* 243: 118282. https://doi.org/10.1016/j.conbuildmat.2020.118282
39. Hashim M, Tantray M (2021) Comparative study on the performance of protein and synthetic-based foaming agents used in foamed concrete. *Case Stud Constr Mater* 14: e00524. https://doi.org/10.1016/j.cscm.2021.e00524
40. Gao M, Li M, Wang J, et al. (2024) Effect of fly ash on properties and hydration of calcium sulphoaluminate cement-based materials with high water content. *De Gruyter Brill* 63: 20240046. https://doi.org/10.1515/rams-2024-0046
41. Lin L, Tao J, Chen B, et al. (2022) Preparation and properties of foamed cement for lightweight thermal insulation with Ti-extraction blast furnace slag and sulfoaluminate cement by chemical foaming. *Constr Build Mater* 337: 127634. https://doi.org/10.1016/j.conbuildmat.2022.127634
42. Behnia S, Jafari A, Soltanpoor W, et al. (2009) Nonlinear transitions of a spherical cavitation bubble. *Chaos Solition Frac* 41: 818–828. https://doi.org/10.1016/j.chaos.2008.04.011
43. Nath P, Sarker P (2011) Effect of fly ash on the durability properties of high strength concrete. *Procedia Eng* 14: 1149–1156. https://doi.org/10.1016/j.proeng.2011.07.144
44. Kang M, Jia Y, Guo P, et al. (2024) Influence of fly ash content on macroscopic properties and microstructure of high-performance concrete. *Res Sq* 14: 3844–3844. https://doi.org/10.21203/rs.3.rs-4821515/v1
45. Aamar D, Ali MM (2021) Influence of cenospheres and fly ash on the mechanical and durability properties of high-performance cement mortar under different curing regimes. *Constr Build Mater* 279: 122458. https://doi.org/10.1016/j.conbuildmat.2021.122458
46. Gao D, Meng Y, Yang L, et al. (2019) Effect of ground granulated blast furnace slag on the properties of calcium sulfoaluminate cement. *Constr Build Mater* 227: 116665. https://doi.org/10.1016/j.conbuildmat.2019.08.046
47. Standard for test methods of basic properties of construction mortar JGJ/T 70-2009. Ministry of Housing and Urban-Rural Development of the People's Republic of China (MOHURD); 2009 [in Chinese]. Available from: https://openstd.samr.gov.cn.

48. Li G, Tan H, He X, et al. (2021) The influence of wet ground fly ash on the performance of foamed concrete. *Constr Build Mater* 304: 124676. https://doi.org/10.1016/j.conbuildmat.2021.124676
49. Libre NA, Khoshnazar R, Shekarchi M (2009) Relationship between fluidity and stability of self-consolidating mortar incorporating chemical and mineral admixtures. *Constr Build Mater* 24: 1262–1271. https://doi.org/10.1016/j.conbuildmat.2009.12.009
50. Zhang T, Ma B, Jiang D, et al. (2021) Comparative research on the effect of various mineral admixtures on the early hydration process of cement. *Constr Build Mater* 301: 124372. https://doi.org/10.1016/j.conbuildmat.2021.124372
51. Azimi AH (2015) Experimental investigations on the physical and rheological characteristics of sand–foam mixtures. *J Non-newton Fluid* 221: 28–39. https://doi.org/10.1016/j.jnnfm.2015.04.003
52. Khan MI (2014) Experimental investigation on mechanical characterization of fiber reinforced foamed concrete. Master's Thesis, University of Akron, Akron, OH, USA.
53. Bentz DP (2007) Internal curing of high-performance blended cement mortars. *J Mater Res* 104: 408–414. https://doi.org/10.14359/18831
54. Bentz DP, Snyder KA (1999) Protected paste volume in concrete: Extension to internal curing using saturated lightweight fine aggregate. *Cem Concr Res* 29: 1863–1867. https://doi.org/10.1016/S0008-8846(99)00178-7
55. Bentz DP, Hansen AS, Guynn JM (2011) Optimization of cement and fly ash particle sizes to produce sustainable concretes. *Cement Concrete Comp* 33: 824–831. https://doi.org/10.1016/j.cemconcomp.2011.04.008
56. Wang H, Long G, Xie Y, et al. (2022) Effects of intense ultraviolet irradiation on drying shrinkage and microstructural characteristics of cement mortar. *Constr Build Mater* 347: 128513. https://doi.org/10.1016/j.conbuildmat.2022.128513
57. Zhang W, Hama Y, Na SH (2015) Drying shrinkage and microstructure characteristics of mortar incorporating ground granulated blast furnace slag and shrinkage reducing admixture. *Constr Build Mater* 93: 267–277. https://doi.org/10.1016/j.conbuildmat.2015.05.103
58. Alnahhal MF, Kim T, Hajimohammadi A (2020) Evolution of flow properties, plastic viscosity, and yield stress of alkali-activated fly ash/slag pastes. *RILEM Tech Lett* 5: 141–149. https://doi.org/10.21809/rilemtechlett.2020.123
59. Hu C, Li H, Liu Z, et al. (2016) Research on properties of foamed concrete reinforced with small sized glazed hollow beads. *Adv Mater Sci Eng* 2016: 5820870. https://doi.org/10.1155/2016/5820870
60. Shahidan S, Aminuddin E, Mohd Noor K, et al. (2017) Potential of hollow glass microsphere as cement replacement for lightweight foam concrete on thermal insulation performance. *MATEC Web Conf* 103: 01014. https://doi.org/10.1051/matecconf/201710301014
61. Gołaszewski J, Klemczak B, Smolana A, et al. (2022) Effect of foaming agent, binder and density on the compressive strength and thermal conductivity of ultra-light foam concrete. *Buildings* 12: 1176. https://doi.org/10.3390/buildings12081176

62. Demirboğa R (2003) Influence of mineral admixtures on thermal conductivity and compressive strength of mortar. *Energy Build* 35: 189–192. https://doi.org/10.1016/S0378-7788(02)00052-X